PCCP

PAPER

Structural analysis of water and carbon tetrachloride adsorbed in activated carbon fibres

Małgorzata Śliwińska-Bartkowiak,[*a] **Henryk Drozdowski,**[a] **Mateusz Kempiński,**[a] **Monika Jażdżewska,**[a] **Yun Long,**[b] **Jeremy C. Palmer**[b] and **Keith E. Gubbins**[b]

We report X-ray diffraction studies of water and carbon tetrachloride adsorbed in nanoporous activated carbon fibres. The fibres are built of turbostratic nanoparticles separated by quasi two-dimensional voids, forming narrow slit-shaped pores. In order to determine the structure of water within the pores and its influence on the fibres' structure, mean interatomic and intermolecular distances have been estimated from the positions of the maxima of the normalized angular distribution functions obtained by X-ray diffraction. We observe a cluster arrangement of the water molecules, as well as significant changes in the interlayer distance of the carbon nanoparticles upon adsorption of both water and carbon tetrachloride. The results suggest that very high pressures arise within the pores, as has been observed in molecular simulations, and this may give rise to the large change in electronic properties of the fibres after adsorption of guest molecules. The in-pore pressure normal to the pore walls is estimated from the experimental data, and is found to be positive and of the order 4000 bar. Molecular simulation results for the normal pressure component are presented for both water and carbon tetrachloride in carbon slit pores, and are in general agreement with the experiments. For both fluids the normal pressure is an oscillating function of pore width.

Introduction

Water confined in a nanoscale environment exhibits unique properties and has been a subject of much attention. Of particular interest have been the effects of confinement on the structure of water and ice in nanopores[1–3] and on dynamical properties of water in one-dimensional, channel-like pores.[4,5]

The phase behaviour of confined water has not been extensively explored. It is frequently observed that phase changes which only occur at high pressures or at low temperatures in the bulk phase take place in the confined phase at pressures that are orders of magnitude lower (bulk phase pressure in equilibrium with the confined phase) and at normal temperatures.[6,7] A familiar example is the vapour–liquid condensation in the confined phase (capillary condensation), but similar phenomena are observed for solid phases. The structure of confined ice has been studied in carbon nanotubes of 0.7–1.5 nm diameter using molecular simulation[8,9] and experiment,[5,10] and provides convincing evidence for the formation of various kinds of ice nanocrystals, including square-gonal ice as ice VIII and ice IX

in nanotubes of small diameters.[11] Similar quasi-high pressure effects due to confinement are observed in chemical reactions in pores. Reactions that only occur at high pressures in the bulk phase occur readily at normal bulk phase pressures in the confined phase as has been observed in experiments[12] and molecular simulations.[13] The origin of these quasi-high pressure effects on the confinement has been attributed to the strong intermolecular forces between the walls of the pores and the molecules of the confined phase (capillary forces, in macroscopic parlance), leading to effective pressures in the pores that are orders of magnitude higher than in the bulk phase.[6,14–17] Our calculations[15,16] show that very high tangential (of the order 10^4 bar or more) and normal (of the order 10^3 bar or more) pressures are expected in carbon micropores and small mesopores. These high in-pore pressures unify a wide range of previously unconnected phenomena, such as the observation of high pressure phases and high pressure reactions in nanoporous materials, and provide a connection between the behaviour of confined and bulk phases at high pressure. Such relations could provide a useful guide to future experimental studies of high pressure phenomena in nanoporous carbons. A further important finding is that relatively small changes in the bulk pressure have a very large effect on the in-pore pressure. Sensitivity to the bulk phase pressure suggests that it should be possible to experimentally observe a range of high pressure phenomena by simply varying the bulk pressure over a small range. This sensitivity also provides

[a] *Faculty of Physics, Adam Mickiewicz University, 61-614 Poznań, Poland. E-mail: msb@amu.edu.pl; Fax: +4861 8295155; Tel: +4861 8295202*
[b] *Department of Chemical and Biomolecular Engineering, North Carolina State University, Raleigh, NC 27695, USA. E-mail: keg@ncsu.edu; Fax: 919 513 2470; Tel: 1 919 513 0481*

This journal is © the Owner Societies 2012

Phys. Chem. Chem. Phys., 2012, **14**, 7145–7153 | 7145

the explanation for the large effect of bulk pressure on the melting curve for confined phases that has been observed in molecular simulations.[14,17] Finally, our results also indicate that for materials with less strongly attractive walls (e.g. silica and many oxides) the pressure enhancement effect is weaker, although still large, while for more strongly attractive walls (e.g. mica) we can expect even larger enhancements.[15]

Recent studies[18] have shown that activated carbon fibres (ACF) are composed of quasi-graphitic particles of nanometre size. Each nanoparticle consists of several defective graphene layers with different spacings from graphite, forming the so-called turbostratic structure. The process of activation causes the development of slit pores—quasi-2D empty voids between the nanoparticles, approximately 1 nm in size. Since these pores are of molecular dimensions, ACF exhibits BET surface areas of up to 3000 m^2 g^{-1} and good adsorption properties for small molecules.[18] The slit shape of the pores in ACF provides the simplest pore geometry for understanding pressure enhancement effects, and facilitates comparisons with molecular simulations.

As reported in previous works, electron paramagnetic resonance (EPR) as well as conductivity measurements show significant changes in the electronic properties of ACF after the adsorption of guest molecules.[19,20] The electronic properties of ACF are characteristic of granular systems with strong localization of charge carriers. Nanoparticles are electrically separated with potential barriers for electron hopping. These barriers, as well as energy levels of the individual nanoparticles, are modified by interactions with the adsorbed molecules. Thus the ACF nanoparticles can be treated as single electron conductors, with the possibility to control the electrical transport through the fibres.[21] As indicated in ref. 22 the stronger interactions between water molecules and pore walls cause greater localization of spins as compared to CCl_4 molecules, and therefore water serves as a more effective medium for controlling the conducting properties of the ACF. Also the so-called Coulomb gap opening is observed in ACF after water adsorption.[23]

In order to further investigate the behaviour of water confined in ACF, we report here structural studies of the ACF–water system. For comparison we present also the behaviour of ACF in response to the adsorption of CCl_4, a fluid of nonpolar, quasi-spherical molecules. The normal component of the pressure tensor in the pores is estimated from the stress-induced structural changes of the ACF, and is found to be a few thousand bars in both cases. We also report molecular simulation studies for these two fluids in a simple model of the ACF material, and show that the normal pressure component is an oscillating function of the pore width. For the particular pore width studied here, $H = 1.4$ nm, the calculated normal pressure is positive and a few thousand bars for both adsorbates, which is in generally good agreement with the experiments.

Experimental

The structure of ACF, ACF–water and ACF–carbon tetrachloride systems was studied at 300 K using X-ray diffraction from a monochromatic source. For each sample, a cuvette with 0.01 mm thick windows of Styroflex foil containing a 3 mm thick layer of the sample was installed in a X-ray goniometer.

Measurements of scattered radiation intensity were performed in a wide range of wave vectors S ($S_{min} = 4.30$ nm^{-1} to $S_{max} = 153.10$ nm^{-1}), with the use of X-ray radiation MoK_α ($\lambda = 0.071069$ nm). The radiation was monochromatized by reflection from the (002) planes of a flat graphite fragment with an angle of monochromatization of $\Theta_m = 6°00.0'$ ($\Delta\Theta_m = 2.2'$). The X-ray diffraction patterns were recorded on a typical X-ray diffractometer equipped with a special cell for measurements of liquids, described by North and Wagner.[24] The scattered X-ray intensity was corrected to include the polarization and absorption factors,[25] and then normalized.[26] Absorption in the cuvette windows was neglected. Small-angle scattering results ($0° < \Theta < 3°$) were extrapolated to the origin of the coordinate system using the second-order functions.

The adsorbent used was an isotropic pitch-based ACF, carbonized at 950 °C, with a mean pore width of 1.4 nm (measured between the planes through the centres of carbon atoms on opposing pore walls) as determined from adsorption data by density functional theory, and supplied by Ad'all Corporation, Japan. Before the adsorption of water, ACF samples were evacuated at 10^{-5} mbar pressure for several hours and heated to 373 K to ensure that the pores were empty.

Molecular simulation model and method

Semi-Grand Canonical Ensemble Monte Carlo (SGCEMC) simulations were carried out (at constant volume, temperature, chemical potential of adsorbate, and number of wall atoms) for intermolecular potentials chosen to model carbon tetrachloride and water, in slit-shaped carbon pores of varying pore width at 300 K and 1 bar bulk pressure. The simulation cell is shown in Fig. 1. The pore walls consist of three graphene layers lying in the xy plane of dimension $L_x = 4.26$ nm, $L_y = 4.18$ nm, and periodic boundary conditions are applied in the x and y directions parallel to the pore walls, so that the pore is infinite in length in these directions, while being of fixed width, H. The carbon atoms are fixed at their lattice positions, so that the system volume is fixed. The pressure tensor, P, of the adsorbate within the pore has two independent components, the pressure P_N ($= P_{zz}$) normal to the pore walls, and the tangential
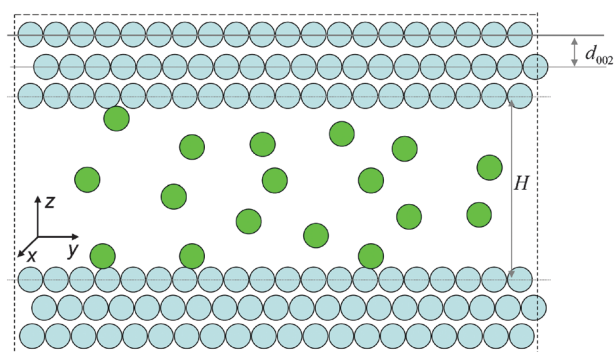
Fig. 1 The simulation cell. The dark (green in color) circles represent adsorbate molecules, and the light (blue in color) circles represent carbon (wall) atoms. Dashed boundaries at each end of the cell indicate periodic boundary conditions. Carbon atoms are shown at reduced scale for clarity.

7146 | *Phys. Chem. Chem. Phys.*, 2012, **14**, 7145–7153

This journal is © the Owner Societies 2012

pressure P_T ($= P_{xx} = P_{yy}$) parallel to the pore walls. The condition of hydrodynamic stability[27] (no net momentum transfer at equilibrium), $\nabla \cdot \boldsymbol{P} = 0$, requires that P_N be a constant, independent of x, y and z in the interior of the pore. As shown by Henderson,[28] the constancy of the chemical potential in the pore, maintained in SGCEMC simulations for a system of constant volume, guarantees that hydrodynamic equilibrium is satisfied.

The normal pressure in the pore can be calculated from the virial route[27] or by the volume perturbation method.[29] For slit shaped pores these two routes have been shown to give results in excellent agreement,[30] and here we use the volume perturbation method. In this method the small changes in the Helmholtz energy, ΔA, due to small changes in the system volume, ΔV, are calculated and the pressure is calculated from:

$$P = -\lim_{\Delta V \to 0} \left(\frac{\Delta A}{\Delta V}\right)_{N,T} = -\left(\frac{\partial A}{\partial V}\right)_{N,T} \quad (1)$$

If the volume change is made by perturbing the length in the direction normal to the wall (z-direction), keeping L_x, L_y constant, the normal component of the pressure can be determined. For the canonical ensemble the relation is:

$$P_N = -\left(\frac{\partial A}{\partial V}\right)_{N,T,L_x,L_y}$$
$$= \rho k_B T - \lim_{\Delta L_z \to 0} \frac{k_B T}{L_x L_y \Delta L_z} \ln \langle e^{-\Delta U/k_B T}\rangle_0 \quad (2)$$

where ρ is the mean number density of the adsorbate in the pore, k_B is the Boltzmann constant, T is the temperature, ΔU is the configurational energy difference between the perturbed and unperturbed systems, and $\langle\ldots\rangle_0$ indicates an ensemble average over the unperturbed system of volume V. For each sampling step, we construct a series of "perturbed" systems by rescaling the z-coordinates of all the atoms by $(1 + \xi)$, where ξ is a small number, and then calculate the thermodynamic normal pressure by the above equation, taking the limiting value as the volume change (as determined by L_z) goes to zero. A series of ξ values ($\pm 10^{-5}, \pm 10^{-6}, \pm 10^{-7}$) are used to calculate the limiting value of P_N as ξ goes to zero.

The simulations were run for 10^8 Monte Carlo configurations to attain equilibrium, and a further 10^8 configurations for the determination of the pressure. The runs were carried out in the semi-grand canonical ensemble, i.e. at constant volume V, with the normal pressure being sampled every 5000 configurations via volume perturbations. The final values of P_N were the result of averaging over 20 000 samples in the unperturbed system of volume V.

The adsorbate–adsorbate (aa) LJ parameters for carbon tetrachloride were taken from Arstila et al.,[31] $\varepsilon_{aa}/k_B = 322.7$ K, $\sigma_{aa} = 0.5947$ nm, while those for carbon were taken from Steele,[32] $\varepsilon_{CC}/k_B = 28.0$ K, $\sigma_{CC} = 0.340$ nm. Parameters for the adsorbate (a)–carbon (C) interactions were calculated from the Lorentz–Berthelot combining rules, $\varepsilon_{aC} = (\varepsilon_{aa}\varepsilon_{CC})^{1/2}$ and $\sigma_{aC} = \frac{1}{2}(\sigma_{aa} + \sigma_{CC})$. Water–water interactions were modelled using the extended simple-point-charge (SPC/E) pair potential.[33] This model consists of a LJ potential centred on the O atom, with parameters $\varepsilon_{aa}/k_B = 78.2$ K, $\sigma_{aa} = 0.31656$ nm, and three point charges, one of $-0.8476e$ on the O and one of $+0.4238e$ on each

of the H atoms. The SPC/E model accounts for the direct electrostatic interactions and includes a polarization correction. The water interaction with the carbon walls consists of two terms, a LJ interaction between the O atom and the C atoms, and a two-body induction interaction. Parameters for the LJ oxygen (a)–carbon (C) interactions were calculated using the Lorentz–Berthelot combining rules. The electric field, E_j, acting on a carbon atom j due to the charges on the O and H atoms of the water molecules also leads to polarization of the carbon atom and an induction interaction U_j, given by:

$$U_j = -\int_0^{E_j} \mathrm{d}\boldsymbol{E}_j \cdot \boldsymbol{\mu}_j = -\int_0^{E_j} \mathrm{d}\boldsymbol{E}_j \cdot \alpha\boldsymbol{E}_j \quad (3)$$

where $\alpha = 1.958 \times 10^{-40}$ C m^2 V^{-1} is the isotropic polarizability of a carbon atom,[34] j is the index of the carbon atoms, and E_j and $\boldsymbol{\mu}_j$ are the vector electric field and dipole acting on the j-th carbon atom due to the charges on all the water molecules. Long-range interactions are cut off at 2 nm. As reported by Perera et al.,[35] simple truncation of the SPC/E potential at a cut-off of at least 1.2 nm produces results very similar to the results where Ewald sums are used to treat long-range Coulomb effects.

According to the intermolecular potential model, the normal pressure of the confined water phase can be decomposed into a kinetic part, $P_{N,kin}(\mathbf{r}) = \rho(\mathbf{r})k_B T$, where $\rho(\mathbf{r})$ is the number density at point $\mathbf{r}$, an adsorbate–adsorbate configurational part (dispersion and Coulombic contributions), and an adsorbate–carbon configurational part (dispersion and induction contributions):

$$P_N = P_{N,kin} + P_{N,aa,disp} + P_{N,aa,coul} + P_{N,aC,disp} + P_{N,aC,ind} \quad (4)$$

For confined carbon tetrachloride, the Coulombic (aa,coul) and induction (aC,ind) terms are absent.

Results and discussion

The normalized angular-distribution functions $I(S)$ (where $S = 4\pi\sin\theta/\lambda$) are presented in Fig. 2–4. The positions of the maxima of these functions were found using the Lagrange polynomials method.[36] In the range 0.90 Å$^{-1} < S < 2.60$ Å^{-1} the peak positions were determined with an accuracy of $\Delta S = \pm 0.01$ Å^{-1}. In the range 2.60 Å$^{-1} < S < 4.50$ Å^{-1} the accuracy was $\Delta S = \pm 0.02$ Å^{-1}, and in the remaining range $\Delta S = \pm 0.03$ Å^{-1}. The positions of the maxima in the angular-distribution functions and the corresponding mean interatomic and intermolecular distances, determined directly from the Bragg equation,[37] are presented in Table 1.

Analysis of intensity distribution functions of scattered radiation shows that they are sensitive to the shape of the examined molecules. From the positions of peaks in the range 0.90 Å$^{-1} < S \leq 6.05$ Å^{-1} it is possible to estimate the average minimal interatomic and intermolecular distances. There is a significant correlation between the positions of the maxima in the angular distribution functions and the internal structure of ACF, ACF + H$_2$O and ACF + CCl$_4$.

Stress-induced deformation in activated carbon fibres

The atomic structure of ACF is similar to that of graphite (Fig. 5), consisting of defective graphene layers arranged in a regular hexagonal pattern. Depending on the manufacturing
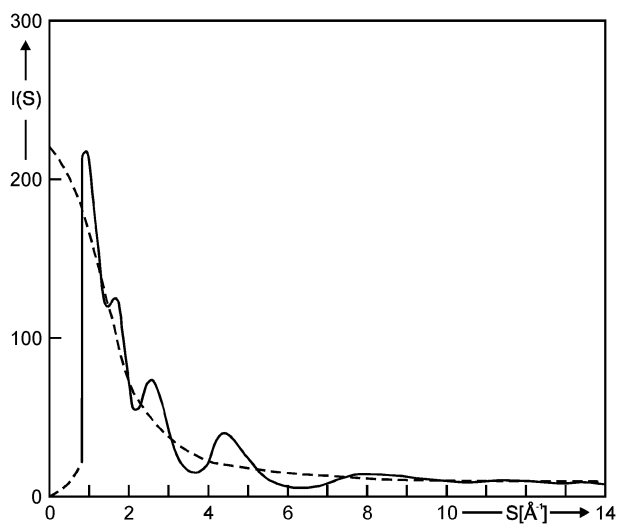
Fig. 2 The normalized, experimental angular distribution curve from X-ray scattering of activated carbon fibres (ACF). The dashed line is the background.
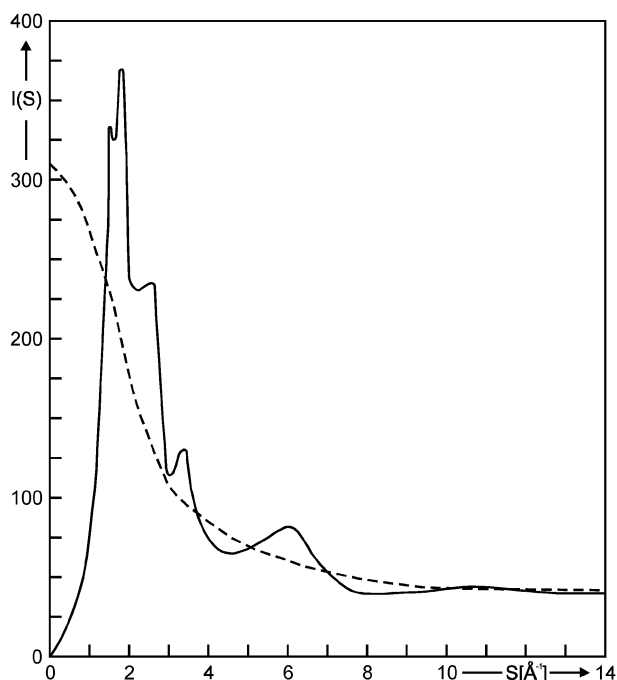
Fig. 3 The normalized experimental angular distribution function from X-ray scattering of ACF with water.

Fig. 4 The normalized experimental angular distribution function from X-ray scattering of ACF with CCl_4.

Table 1 Positions of maxima $S\,(\text{Å}^{-1})$ of angular-distribution functions of ACF, ACF with water and ACF with CCl_4, and corresponding mean interatomic and intermolecular Bragg distances, $d\,(\text{Å})$

Sample	$S/\text{Å}^{-1}$	$D/\text{Å}$
ACF	0.93	8.01
	1.66	**3.78**
	2.58	2.45
	4.40	1.42
ACF + H_2O	1.79	3.52
	1.91	**3.30**
	2.77	2.27
	3.43	1.83
	6.05	1.03
ACF + CCl_4	0.93	8.01
	1.25	6.28
	1.91	**3.33**
	2.23	2.83
	3.13	2.50
	5.25	1.50
	7.20	1.09
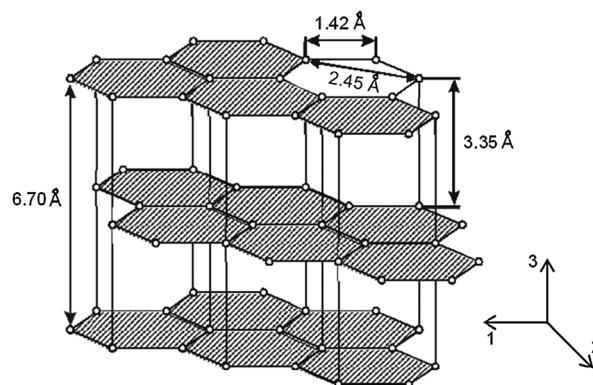
Fig. 5 The structure of graphite.

processes, the graphene planes in carbon fibres may be either turbostratic, graphitic or exhibit a hybrid structure. In graphitic crystalline regions, the layers are stacked parallel to one another in a regular fashion. The atoms within a plane are covalently bonded with an sp^2 hybridization, while the interaction between the sheets occurs through relatively weak van der Waals forces, giving rise to a d-spacing between two graphene layers (d_{002}) in graphite of about 0.335 nm for a single crystal. The Young's moduli of these single crystals have been calculated: longitudinal modulus, E_L (parallel to the basal plane), and transverse compressive modulus, E_T (normal to the basal plane), are 1060 GPa and 36.5 Pa, respectively.[38,39] Thus the transverse compressive modulus is 29.0 times smaller than the longitudinal one.

The basic structural unit of many carbon fibres consists of a stack of turbostratic layers, where the parallel graphene sheets are stacked irregularly or are randomly folded. It has been reported[18] that the irregular stacking and the presence of sp^3 bonding can increase d-spacing. As follows from the experimental results for the Bragg positions (Table 1), ACF's graphitic
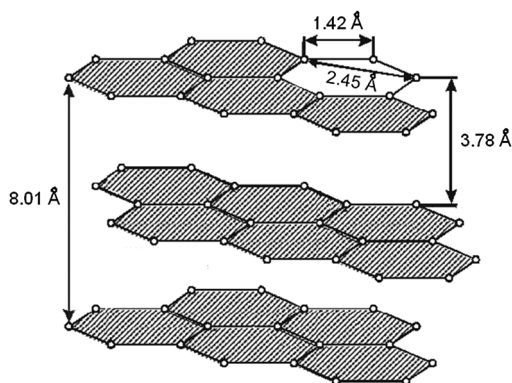
Fig. 6 Interatomic distances in a single ACF nanoparticle.

nanoparticle structure (basic structural unit—BSU) can be shown schematically in Fig. 6 with denoted distances.

The interplanar distance in ACF was found to be 3.78 Å but is observed to change after adsorption to a smaller value more characteristic of bulk graphite (from 3.78 Å to 3.30 Å for water, and 3.78 Å to 3.33 Å for carbon tetrachloride, Table 1). Such shrinkage of interplanar distances in ACF, when hydrophobic nanographite particles are surrounded by water molecules, has been observed before, and is accompanied by a suppression of paramagnetism.[40] The low spin state is a consequence of the internal pressure of adsorbed molecules, which causes the nanographites to shrink. This result is in good agreement with the change of the lattice constant observed in our experiment. The results point to the possibility of deformation of the carbon hexagons that make up the graphene sheets which results in a reduction of the C_1–C_3 bond length from 2.45 Å to 2.27 Å.

The observed shrinkage in the interplanar distance in ACF results from the enhanced pressure normal to the pore walls, P_N. This in-pore pressure can be roughly estimated using Young's equation, $P_N = E_T(\Delta d_{002}/d_{002})$, provided that the transverse compressive modulus E_T is known. Here Δd_{002} is the change in the interlayer spacing of graphene sheets due to the adsorbed nano-phase. A number of measurements have been reported for both the longitudinal, E_L, and transverse moduli, E_T, for ACF. Their values depend strongly on the precursor used, the method of preparation and the temperature of carbonization.[41–48] Although measurements of the transverse compressive modulus are not available for the ACF used here, an estimate of its value can be made from measurements on similar pitch-based carbon fibres. Kawabata[43] reports values of E_T for three closely related pitch-based carbon fibres of 3.08, 4.07 and 4.85 GPa. This suggests a value of E_T of about 4.0 GPa. Kawabata[48] and also Peebles et al.[44] report values of E_T for two PAN-based fibres of 3.2 and 4.0 GPa. However, for fibres carbonized at 950 °C it is known that the moduli for PAN-based are approximately two times larger than those for pitch-based fibres.[41,44] This suggests a value of E_T for our pitch-based carbon of about 1.8 GPa. Here we take the value of E_T for our ACF to be 2.9 GPa, the average of the above two values, 4.0 and 1.8. While a rough estimate, the value 2.9 GPa for E_T is consistent with what is known of the values of the longitudinal modulus, E_L, for pitch-based fibres. For example, Peebles et al.[44] and Matsumoto[41] report values of E_L of about 100 GPa for pitch-based fibres heat treated at 950 °C. If we

assume that E_T is 29 times smaller than E_L, as is the case for graphite, we obtain a value of $E_T = 3.4$ GPa, which is in reasonable agreement with the above value of 2.9.

The shrinkage in the interplanar distance in ACF due to water adsorption is from 3.78 Å to 3.30 Å (see Fig. 5 and Table 1), so that $(\Delta d_{002}/d_{002}) = 0.48/3.78 \approx 0.13$. Thus we can estimate the approximate magnitude of the normal pressure in ACF under water adsorption conditions as $P_N = 0.13 \times 2.9$ GPa, or 377 MPa.

For the adsorption of CCl_4, the interplanar distance of ACF shrinks from 3.78 to 3.33 Å, and the normal pressure is estimated to be $P_N = (0.45/3.78)2.9 = 345$ MPa. Clearly, these pressures are rough estimates, with error bars of perhaps ±50%.

The simulation results for the normal pressure of LJ carbon tetrachloride and SPC/E water are shown in Fig. 7 as a function of the pore width for experimental conditions (bulk pressure of 1 bar and temperature of 300 K). The pore width H is defined as the distance between the center planes of carbon atoms on the opposing walls of the pore. For a pore width of 1.4 nm, the simulated normal pressures for carbon tetrachloride and water are 284 MPa and 490 MPa, respectively, and are in qualitative agreement with the estimated value from the experiment (345 ± 173 MPa and 377 ± 189 MPa, respectively). In Fig. 7c the effective pore width, $H' = H - \sigma_{CC}$, is used, which takes account of the dead space near the pore walls. The dimensionless accessible pore width, H'^*, used in Fig. 7c, gives the approximate number of complete adsorbed layers in the slit pore. In the case of water, the LJ parameters of the oxygen site of water[33] were used: $\varepsilon_{aa}/k_B = 78.2$ K, $\sigma_{aa} = 0.31656$ nm. While the LJ potential is clearly a very crude approximation for water, we expect that the size parameter of oxygen gives a rough estimate of the molecule's diameter. The oscillations in P_N with pore width have been observed in surface force measurements[49,50] and also in molecular simulations and density functional theory calculations,[51] and arise from oscillations in the mean density in the pore on increasing H as new adsorbed layers form.[16] The positive and negative oscillations of P_N in the case of CCl_4 indicate that the system is in compression (average intermolecular separations near the wall in the positive, repulsive region of the intermolecular pair force) and tension (average intermolecular separations near the wall in the negative, attractive region of the intermolecular pair force), respectively. For water, except for very small pore widths ($H < 0.82$ nm), P_N is always positive, which is a result of the non-wetting nature of water (the water–carbon interaction is weak relative to the water–water interaction). This phenomenon was also observed in experiments on water using the surface force apparatus.[52] From Fig. 7c we see that the oscillations for water and carbon tetrachloride are almost in phase, as expected, but the amplitudes of the P_N oscillations, while of the order of a few hundred MPa, are somewhat different. This is to be expected since P_N depends on the value of the microscopic wetting parameter, α_w, which measures the strength of the adsorbate–wall interaction relative to the adsorbate–adsorbate interaction, and α_w takes different values for carbon tetrachloride and water.[53]

In Fig. 8 are shown the individual contributions (see eqn (4)), averaged over the accessible pore width, H', to the normal pressure of carbon tetrachloride and water. Fig 8a shows the kinetic and configurational (adsorbate–carbon and adsorbate–adsorbate

This journal is © the Owner Societies 2012

Phys. Chem. Chem. Phys., 2012, **14**, 7145–7153 | 7149
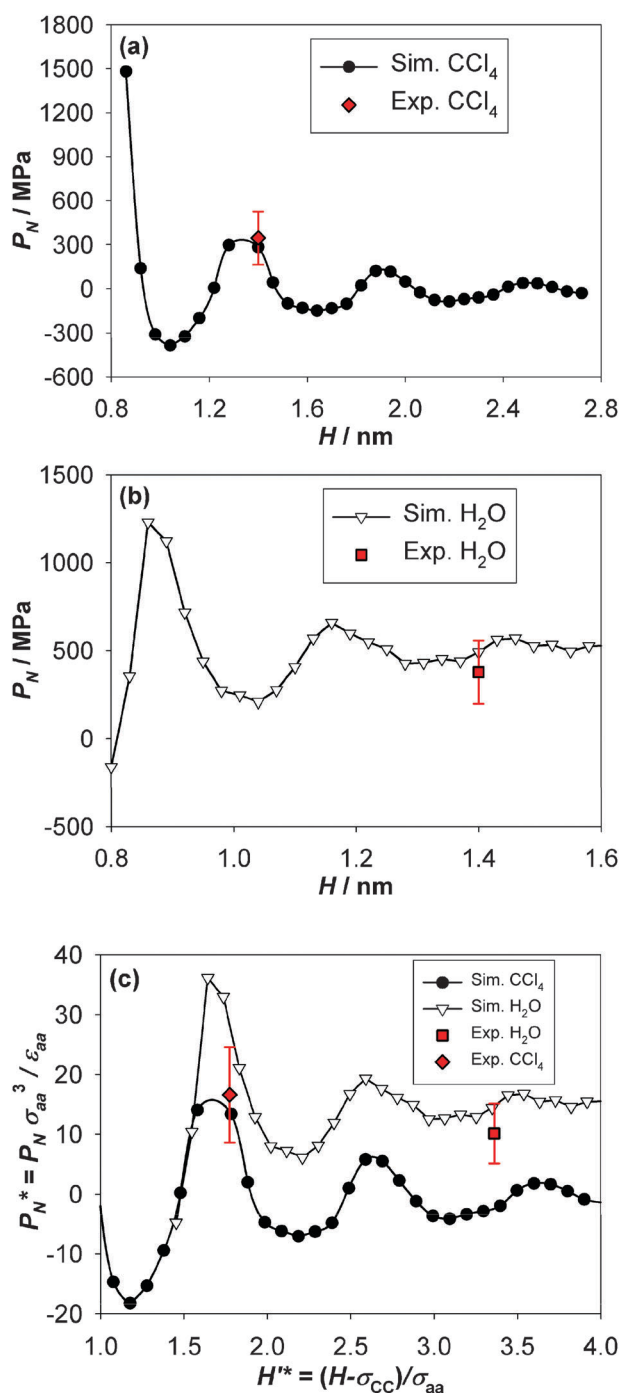
Fig. 7 Simulation results for the normal pressure of (a) CCl$_4$ and (b) water, each in dimensional units, and (c) in dimensionless units for CCl$_4$ and water at 300 K adsorbed in slit carbon pores of different widths. The bulk phase pressure is 1 bar. The experimental results for the pore width of 1.4 nm are also included.

dispersion) contributions to the normal pressure of confined carbon tetrachloride. The kinetic part decreases with increasing pore width, because the in-pore density of the adsorbate decreases in larger pores as the influence of the adsorbate–carbon attractive interaction becomes less. The adsorbate–adsorbate dispersion contribution is oscillating with a period of ∼0.6 nm (the diameter of the CCl$_4$ molecule), as expected, and is positive or negative

depending on pore width. This is because the LJ adsorbate molecules form an integer number of well defined layers in the slit pore; the pore width must increase by about 0.6 nm to accommodate an additional layer, leading to an oscillation in mean density, and hence in P_N, as H increases. The adsorbate–carbon dispersion contribution is also oscillating, but is negative except for pore widths H smaller than 0.92 nm, below which the molecules have increasing difficulty to enter the pore (increasingly repulsive adsorbate–wall interactions).
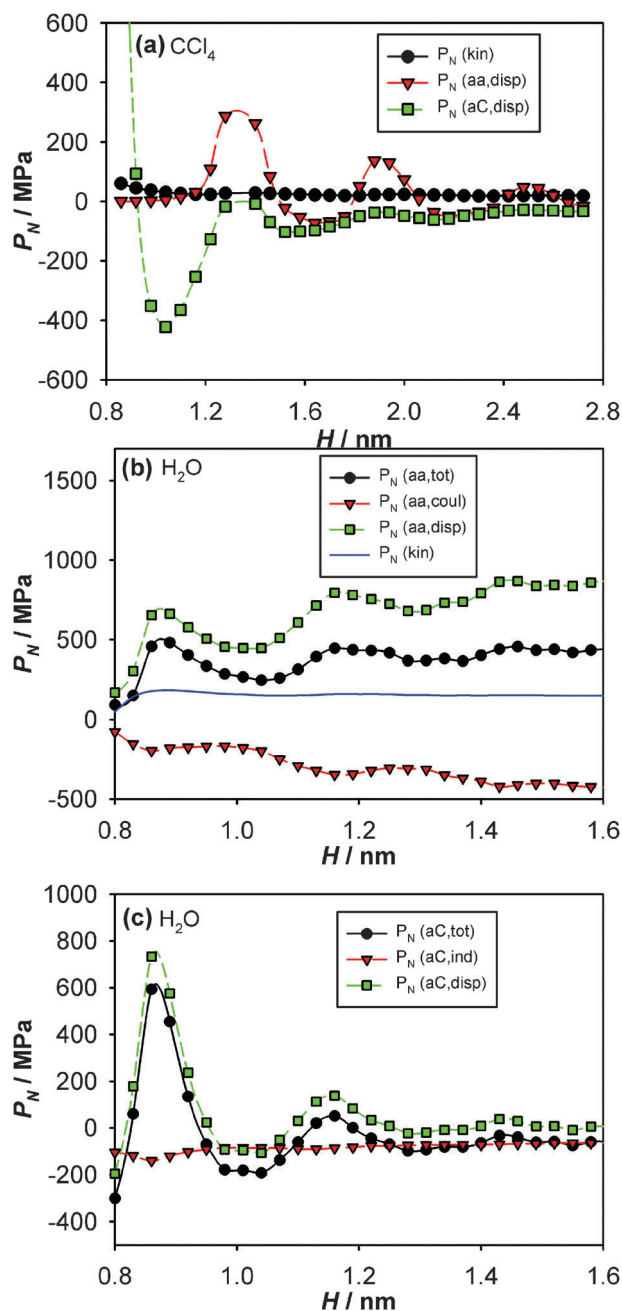
Fig. 8 Individual contributions to the normal pressure of CCl$_4$ and water *vs.* pore width at 300 K and 1 bar bulk phase pressure, from molecular simulation: (a) CCl$_4$; (b) H$_2$O, kinetic and configurational (Coulombic, dispersion and total) contributions from water–water (aa) interactions; and (c) H$_2$O, configurational contributions (induction, dispersion and total) from water–carbon (aC) interactions.

7150 | *Phys. Chem. Chem. Phys.*, 2012, **14**, 7145–7153

This journal is © the Owner Societies 2012

The individual contributions to the normal pressure of water are shown in Fig. 8b and c. Except for pore widths below $H \approx 0.86$ nm (where water molecules can no longer form two layers, leading to lower densities), the kinetic contribution (Fig. 8b) decreases slightly with increasing pore width, having values from 170 to 150 MPa, because the average in-pore density decreases as the pore becomes wider. The adsorbate–adsorbate configurational contributions (dispersion (LJ) and Coulombic) are also shown in Fig. 8b. The overall adsorbate–adsorbate contribution is positive and oscillates with decreasing amplitude as pore width increases. The dispersion part of the water–water contribution oscillates around an increasing line, suggesting that the separation distance between the oxygen sites in water molecules decreases with increasing pore width. This increasing pressure contribution is compensated by the decrease in the contribution from the Coulombic interactions between charges in water molecules. These trends with increasing H are believed to be due to the fact that in larger pores water molecules have more space to arrange and orient themselves, and adopt more close-packed and energetically favourable configurations. The adsorbate–carbon configurational contributions for water are shown in Fig. 8c. As expected, the dispersion part oscillates due to layering effects, but with decreasing amplitude, because the interaction with the wall becomes weaker as the pore width increases. The induction contribution is negative and gets slowly weaker with increasing pore width.

Water structure in activated carbon fibres

In the angular distribution function for ACF with water, shown in Fig. 2, there is a clear peak for $S_4 = 1.79$ Å^{-1}, which corresponds to $d = 3.52$ Å. The typical structure of a water molecule is presented in Fig. 9a and its diameter is approximately 3.25 Å. The electron configuration of the oxygen atom determines the spatial structure of the molecule. The angle between O–H bonds is approximately 105°. The strong dipole moment of water is the result of the dipole moment of the O–H bonds. In the case of an isolated water molecule the total dipole moment equals 1.85 D (6.18×10^{-30} C m), while the O–H dipole moment equals 1.52 D (5.074×10^{-30} C m).[54]

The above data, together with the assumed geometrical model of the molecule presented in Fig. 9a, provide the basis for proposing the arrangement of water molecules presented in Fig. 9b, with the first coordination sphere equal to 4, which is typical for isolated water molecules. The angular distribution function for ACF with water presented in Fig. 3 has a clear peak for $S_4 = 3.43$ Å^{-1}, which corresponds to $d = 1.83$ Å. It provides evidence for the existence of O–H hydrogen bonds between the two neighbouring molecules and is consistent with Pauling data.[55]

Molecular simulation studies of the structure and stability of the water clusters[56] suggest that at low temperatures (or high pressure) $(H_2O)_8$ can stabilize into a cube with D_{2d} or S_4 symmetry and that, at higher temperatures, entropy considerations may favour other geometries. Experiments involving pure water clusters[57] as well as hydrated molecules[58] support the cubic structure for the octamer shown in Fig. 10. The most stable geometry of $(H_2O)_8$ is cubic with D_{2d} symmetry, and thus the dipole moment is 0, with a hydrogen bond length,
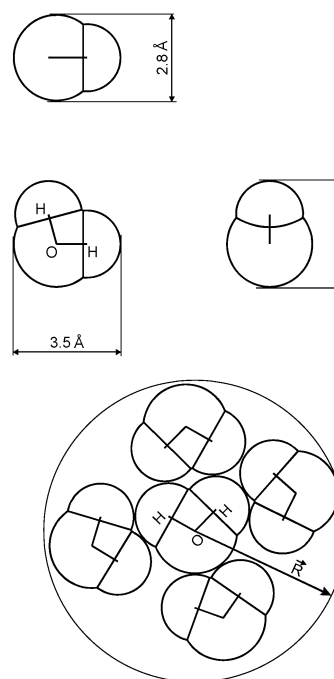
Fig. 9 Water molecule. (a) Geometrical model of an isolated water molecule. (b) Water molecule arrangement ($\vec{R}$ represents the radius of the first coordination sphere).
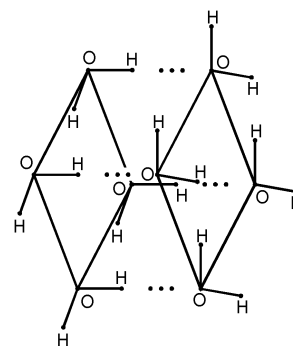
Fig. 10 Water molecules forming a cubic cluster.

r_{OH}, of about 1.80 Å and r_{OO} of 2.73 Å. Considering the data in Table 1 along with this approximate model of molecular arrangement, we can propose that water forms into cubic clusters containing eight molecules and that such water clusters can form in slit shaped pores of ACF that are ∼1.4 nm in width.

In addition, the pressure enhancement in these pores leads to the shrinkage of the interlayer distance in ACF and can stabilize the cubic clusters of water within the ACF pores. The water monomers observed in the system are related to the excess bulk water in the sample, as the ACF nanoparticles are suspended in water. Our previous studies of the melting behaviour of water confined in ACF showed that the melting point of water in pores is 246 K,[59] and the ice in pores has a hexagonal form, I_h. We note that the melting point for bulk ice I_h under a pressure of 238 MPa is 249 K,[60] which is consistent with a pressure of the order of hundreds of MPa in ACF pores.

Discussion and conclusions

We have used MoK$_\alpha$ short-wave radiation to determine the shortest interatomic and intermolecular distances of activated carbon fibres (ACF), and ACF with water and with carbon tetrachloride. From these results we show that adsorption causes significant changes of the lattice constants in the graphitic structure of ACF nanocrystallites, suggesting the existence of high pressures within the pores. Using the elastic modulus of ACF, we estimate the value of the normal pressure in the pores to be on the order of a few hundred MPa for the liquids studied. We have also carried out GCMC simulations for water and carbon tetrachloride in simple slit-pore carbon models of ACF. The calculated normal pressure component oscillates as the pore width is increased, as has been observed in surface force experiments. From the experimental studies we estimate the pressure normal to the pore walls to be 377 $\pm$ 189 MPa for water and 345 $\pm$ 173 MPa for carbon tetrachloride. These can be compared with the simulation results: 490 MPa for water and 284 MPa for carbon tetrachloride for an experimental pore width of 1.4 nm, in qualitative agreement with experiment. The principal uncertainty in the experimental estimates of P_N is from the uncertainty in the value of the transverse compressive elastic modulus of the ACF.

The molecular simulations make it possible to identify the contribution of the various kinetic and configurational terms to the pressure. The kinetic contribution (resulting from the molecular momenta) to the normal pressure is always positive and relatively small, whereas the configurational contributions (resulting from intermolecular forces) can be positive or negative. For carbon tetrachloride the contribution from CCl$_4$–carbon interactions is negative, except for very small pore widths in the molecular sieving region, whereas the contribution from CCl$_4$–CCl$_4$ interactions is positive for most pore widths, and oscillates with increasing H. For water the contribution to P_N from water–water interactions is positive for all pore widths, with a positive contribution from dispersion interactions outweighing the negative contribution from the Coulomb interactions between charges on the water molecules. The contribution from water–carbon interactions oscillates with increasing pore width, being positive or negative depending on the pore width. The contribution from water–carbon dispersion interactions oscillates similarly, while the induction interaction contribution is negative, and is of the order -100 MPa for pore widths of up to about 1.3 nm.

Further evidence for high pressures in water confined in carbons having cylindrical pores (single walled carbon nanotubes and CMK carbons) is provided by recent experimental neutron diffraction studies[61,62] carried out at lower temperatures, which suggest the presence of nano-crystals of ice VIII and ice IX. For bulk water these phases are observed only at pressures of above 200 MPa (ice IX) and above 1 GPa (ice VIII). It is likely that in these phenomena the tangential pressure[15,16] plays a prominent role, in addition to the normal pressure in the pores.

Liquid water adsorbed in the ACF pores consists of clusters formed from hydrogen-bonded molecules, with disordered areas where there are fewer or no hydrogen bonds. The mean distance between the free water molecules (non-clustered) is approximately 3.5 Å. We suggest the existence of cubic clusters composed of eight water molecules bonded with 1.83 Å hydrogen bonds in ACF pores, a consequence of pressure enhancement in the pores.

Notes and references

1 A. Striolo, A. A. Chialvo, K. E. Gubbins and P. T. Cummings, *J. Chem. Phys.*, 2005, **122**, 234712.
2 A. I. Kolesnikov, J. M. Zanotti, C. K. Lonng, P. Thiyagarajan, A. P. Moravsky, R. O. Loufty and C. J. Burnham, *Phys. Rev. Lett.*, 1999, **93**, 035503.
3 H. Tanaka and K. Koga, *J. Chem. Phys.*, 2005, **123**, 094706.
4 J. Zheng, E. M. Lemmon, H. A. Tsao, H. J. Sheng and S. Jiag, *J. Chem. Phys.*, 2005, **122**, 214702.
5 K. Matsuda, T. Hibi, H. Kadowaki, H. Kataura and Y. Maniwa, *Phys. Rev. B: Condens. Matter Mater. Phys.*, 2006, **74**, 073415.
6 L. D. Gelb, K. E. Gubbins, R. Radhakrishnan and M. Sliwinska-Bartkowiak, *Rep. Prog. Phys.*, 1999, **62**, 1573.
7 C. Alba-Simonesco, B. Coasne, G. Dudziak, K. E. Gubbins, R. Radhakrishnan and M. Sliwinska-Bartkowiak, *J. Phys.: Condens. Matter*, 2006, **18**, R14.
8 K. Koga, G. T. Gao, H. Tanaka and X. C. Zeng, *Nature*, 2001, **412**, 802.
9 J. Bai, J. Wang and X. C. Zeng, *Proc. Natl. Acad. Sci. U. S. A.*, 2006, **183**, 19664.
10 D. Takaiwa, I. Hatano, K. Koga and H. Tanaka, *Proc. Natl. Acad. Sci. U. S. A.*, 2008, **105**, 39.
11 M. Jażdżewska, M. Śliwińska-Bartkowiak, A. I. Beskrovnyy, S. G. Vasilovskiy, S.-W. Ting, K. Y. Chan, L. Huang and K. E. Gubbins, *Phys. Chem. Chem. Phys.*, 2011, **13**, 9008.
12 K. Kaneko, N. Fukuzaki, K. Kakei, T. Suzuki and S. Ozeki, *Langmuir*, 1989, **5**, 960; J. Imai, M. Souma, S. Ozeki, T. Suzuki and K. Kaneko, *J. Phys. Chem.*, 1991, **95**, 9955; Y. Nishi, T. Suzuki and K. Kaneko, *J. Phys. Chem. B*, 1997, **101**, 1938.
13 C. H. Turner, J. K. Johnson and K. E. Gubbins, *J. Chem. Phys.*, 2001, **114**, 1851.
14 M. Miyahara, H. Kanda, M. Shibao and K. Higashitani, *J. Chem. Phys.*, 2000, **112**, 9909.
15 Y. Long, J. Palmer, B. Coasne, M. Sliwinska-Bartkowiak and K. E. Gubbins, *Microporous Mesoporous Mater.*, 2012, **154**, 19.
16 Y. Long, J. Palmer, B. Coasne, M. Sliwinska-Bartkowiak and K. E. Gubbins, *Phys. Chem. Chem. Phys.*, 2011, **13**, 17163.
17 B. Coasne, J. Czwartos, M. Sliwinska-Bartkowiak and K. E. Gubbins, *J. Phys. Chem. B*, 2009, **113**, 13874.
18 A. M. Rao, A. W. P. Fung, M. S. Dresselhaus and M. Endo, *J. Mater. Res.*, 1992, **7**, 1788.
19 M. Kempiński, M. Śliwińska-Bartkowiak and W. Kempiński, *Mol. Phys. Rep.*, 2003, **37**, 136.
20 M. Kempiński, W. Kempiński and M. Śliwińska-Bartkowiak, *Rev. Adv. Mater. Sci.*, 2006, **12**, 72.
21 M. Kempiński, W. Kempiński, J. Kaszyński and M. Śliwińska-Bartkowiak, *Appl. Phys. Lett.*, 2006, **88**, 143103.
22 M. Kempiński, M. Śliwińska-Bartkowiak and W. Kempiński, *Rev. Adv. Mater. Sci.*, 2007, **14**, 163.
23 S. Lijewski, M. Wencka, S. K. Hoffmann, M. Kempiński, W. Kempiński and M. Śliwińska-Bartkowiak, *Phys. Rev. B: Condens. Matter Mater. Phys.*, 2008, **77**, 014304.
24 D. M. North and C. N. J. Wagner, *J. Appl. Crystallogr.*, 1969, **2**, 149.
25 K. Sagel, *Tabellen zur Röntgenstrukturanalyse*, Springer, Berlin, 1958.

26 J. Krogh-Moe, *Acta Crystallogr.*, 1956, **9**, 951; N. Norman, *Acta Crystallogr.*, 1957, **10**, 370.

27 C. G. Gray, K. E. Gubbins and C. G. Joslin, *Theory of Molecular Fluids. 2. Applications, Sec. 8.3*, Oxford University Press, Oxford, 2011.

28 J. R. Henderson, *Mol. Phys.*, 1983, **48**, 715. See also: A. Z. Panagiotopoulos, *Mol. Phys.*, 1987, **62**, 701.

29 E. de Miguel and G. Jackson, *Mol. Phys.*, 2006, **104**, 717.

30 Y. Long and K. E. Gubbins, to be published, 2012.

31 H. Arstila, O. V. Vasilev and M. Kulmala, *J. Chem. Phys.*, 1997, **107**, 544–549.

32 W. A. Steele, *Surf. Sci.*, 1973, **36**, 317.

33 H. J. C. Berendsen, J. R. Grigera and T. P. Straatsma, *J. Phys. Chem.*, 1986, **91**, 6269.

34 T. M. Miller and B. Bederson, *Adv. At. Mol. Phys.*, 1977, **13**, 1.

35 L. Perera, U. Essmann and M. L. Berkowitz, *J. Chem. Phys.*, 1995, **102**, 450.

36 H. P. Klug and L. E. Alexander, *X-Ray Diffraction Procedures for Polycrystalline and Amorphous Materials*, Wiley, New York–London, 1974.

37 H. N. V. Temperley and D. H. Trevena, *Liquids and their Properties*, Ellis Horwood, Chichester, 1978.

38 O. L. Blakslee, *J. Appl. Phys.*, 1970, **41**, 3373.

39 E. J. Seldin and C. W. Nezbeda, *J. Appl. Phys.*, 1970, **41**, 3389.

40 H. Sato, N. Kawatsu, T. Enoki, M. Endo, R. Kobori, S. Maruyama and K. Kaneko, *Solid State Commun.*, 2003, **125**, 641.

41 T. Matsumoto, *Pure Appl. Chem.*, 1985, **57**, 1553.

42 K. Takahashi and T.-W. Chou, *Metall. Trans. A*, 1988, **19**, 129.

43 S. Kawabata, *J. Text. Inst.*, 1990, **81**, 432.

44 L. H. Peebles, Y. G. Yanovsky, A. G. Sirota, V. V. Bogdanov and P. M. Levit, in *Carbon Fibers*, ed. J. -B. Donnet, T. K. Wang, J. C. M. Peng and S. Rebouilllat, Marcel Dekker, New York, 3rd edn, 1988, p. 311.

45 C. Sauder, J. Lamon and R. Pailler, *Carbon*, 2004, **42**, 715.

46 X. Huang, *Materials*, 2009, **2**, 2369.

47 The Japan Carbon Fibers Manufacturers' Association. http://www.carbonfiber.gr.jp/english/faq/faq.htm.

48 S. Kawabata, *Proc. 4th Japan-U.S. Conf. on Composite Materials*, Technomic Press, Lancaster, PA, 1988, p. 253.

49 J. Klein and E. Kumacheva, *Science*, 1995, **269**, 816–819.

50 J. Klein and E. Kumacheva, *J. Chem. Phys.*, 1998, **108**, 6996–7009.

51 P. B. Balbuena, D. Berry and K. E. Gubbins, *J. Phys. Chem.*, 1993, **97**, 937–943.

52 U. Raviv, P. Laurat and J. Klein, *J. Chem. Phys.*, 2002, **116**, 5167.

53 R. Radhakrishnan, K. E. Gubbins and M. Sliwinska-Bartkowiak, *J. Chem. Phys.*, 2002, **116**, 1147.

54 S. A. Clough, Y. Beers, G. P. Klein and L. S. Rothman, *J. Chem. Phys.*, 1973, **59**, 2254.

55 L. Pauling and P. Pauling, *Chemistry*, W.H. Freeman and Company, San Francisco, 1985.

56 S. Maheshwary, N. Patel, N. Sathyamurthy, A. Kulkarni and S. R. Gadre, *J. Phys. Chem. A*, 2001, **105**, 10525.

57 U. Buck, I. Ettischer, M. Melzer, V. Buch and V. Sadlej, *Phys. Rev. Lett.*, 1998, **80**, 2578.

58 C. Lee, H. Chen and G. Fitzgerald, *J. Chem. Phys.*, 1995, **102**, 1266.

59 M. Śliwińska-Bartkowiak, G. Dudziak, R. Radhakrishnan and K. E. Gubbins, *Phys. Chem. Chem. Phys.*, 2002, **13**, 2002.

60 O. Schluter, *Impact of High Pressure and Low Temperature Processes on Cellular Materials*, Thesis, Technische Universität Berlin, 2003.

61 M. Sliwinska-Bartkowiak, M. Jazdzewska, L. Huang and K. E. Gubbins, *Phys. Chem. Chem. Phys.*, 2008, **10**, 4996.

62 M. Jazdzewska, M. Sliwinska-Bartkowiak, J. C. Palmer and K. E. Gubbins, paper in preparation.

This journal is © the Owner Societies 2012

Phys. Chem. Chem. Phys., 2012, **14**, 7145–7153 | 7153